Summer generation of the Southern Gulf of California eddy train

Luis Zamudio,[1] Patrick Hogan,[2] and E. Joseph Metzger[2]

[1] Ocean color and sea surface temperature satellite-observations show the existence of a series of anticyclonic eddies along the axis of the southern Gulf of California (SGOC). To investigate the summer generation of these eddies, a regional version of the HYbrid Coordinate Ocean Model (HYCOM) has been configured for the GOC and has been nested inside the global model. A suite of experiments, using the nested GOC model, was developed and used to isolate the effects of the local wind and the effects of the oceanic remote forcing on the generation of the SGOC eddies. The results indicate that the local wind is not essential for the generation of these eddies rather it is the oceanic remote forcing. In the SGOC the monthly variability of the currents and sea surface height is mainly due to the deterministic near-coastal poleward eastern boundary currents (PEBC). The interaction of the PEBC with the topographic irregularities (the capes at Topolobampo and Cabo Lobos and the ridges extending offshore from the entrance of the San Lorenzo and Sinaloa Rivers) generates the SGOC eddies. The northward upper-ocean transport induced by the PEBC includes two maximums, one in May-June and the other in December. During the summers of 1999 and 2004 the PEBC were intensified by the arrival of equatorially-originated downwelling coastally-trapped-waves (CTWs), which contributed to the generation of the SGOC eddies. The summer 2004 CTW increased the northward upper-ocean transport by ~2 Sv. This particular CTW was measured by several tide gauges located along the coast.

1. Introduction

[2] Previous studies have reported the connectivity of the Gulf of California (GOC) with the Pacific Ocean using sea level measurements (from inside and outside of the GOC), hydrographic measurements, analytic-observational models, regional numerical ocean models, and basin-scale and quasi-global numerical ocean models [*Christensen et al.*, 1983; *Enfield and Allen*, 1983; *Baumgartner and Christensen*, 1985; *Badan-Dangon et al.*, 1985; *Bray*, 1988; *Merrifield and Winant*, 1989; *Paden et al.*, 1991; *Merrifield*, 1992; *Ripa*, 1997; *Beier*, 1997; *Beier and Ripa*, 1999; *Castro et al.*, 2000; *Palacios et al.*, 2002; *Zamudio et al.*, 2002; *Marinone*, 2003; *Mascareñas et al.*, 2004; *Martinez and Allen*, 2004a, 2004b; *López et al.*, 2005; *Castro et al.*, 2006; *Palacios-Hernández et al.*, 2006]. In spite of the well accepted importance of the Pacific Ocean forcing on the monthly, annual, and interannual variability of the GOC, an observational-based and/or numerical monthly climatology of the currents at the entrance of the GOC has not been reported.

[3] Documented here is a monthly climatology of the GOC that was simulated with a Pacific configuration of HYCOM. Thus, by nature, this climatology incorporates the climatological ocean response of the GOC to the local and remote forcings and consequently it includes the oceanic remotely-forced summer-generated Southern GOC (SGOC) eddy train (Section 3.1). This climatology can be used as a provider of oceanic boundary conditions for regional models of the GOC. However, if the particular processes to study (e. g. ocean response to hurricanes, upwelling/downwelling events, propagation of CTWs, and/or the generation of specific eddies) are forced by particular local and/or remote forcing events; then, that specific forcing will not be included in any climatological boundary conditions. Hence, in this study, the GOC has been nested in a global version of HYCOM, which provides daily boundary conditions (including specific oceanic forcings) for the regional GOC models.

[4] The summer SGOC eddy train has already been observed in SeaWiFS chlorophyll images during the summer of 1999 [*Pegau et al.*, 2002], and in Modular Ocean Data Assimilation System (MODAS) sea surface temperature (SST) data during the summer of 2004 (Section 3.2). The existence of the satellite-observed SGOC eddies during August 2004 has been corroborated by the direct hydrographic observations of *Castro et al.* [2007]. Also, analyzing observations from drifters, *Lavín et al.* [2007] reported poleward surface currents with maximums of up to 80 cm/s,

[1]Center for Ocean-Atmospheric Prediction Studies, Florida State University, Tallahassee, Florida, USA.
[2]Naval Research Laboratory, Stennis Space Center, Mississippi, USA.

flowing along the eastern coast of the SGOC during June 2004. A month later, the coastal currents weakened and eddies become more evident, and by August 2004 eddies dominated the circulation in the SGOC. Some of the features of the SGOC eddies reported by the authors are surface currents of ~25–50 cm/s, rotation period of ~3–5 days, and eddies' signature to depths of up to 1000 m.

[5] What is the forcing of these eddies? Are these local eddies due to the local and/or remote forcing? Here it is investigated the link between the generation of the summer of 2004 observed eddies and the specific eddy forcing. Two hypothesis are presented and discussed. The first hypothesis is that the local wind is the essential generator of the observed eddies, whereas the second hypothesis implies it oceanic remote forcing.

2. Model

[6] The HYbrid Coordinate Ocean Model (HYCOM) is a hydrostatic primitive equation ocean general circulation model equipped with a hybrid vertical coordinate. HYCOM uses isopycnal (density tracking) coordinates in the open stratified ocean, but reverts to sigma (terrain-following) coordinates in shallow waters regions, and z-level (constant fixed depths) coordinates in the mixed layer and unstratified regions. HYCOM [*Bleck*, 2002] was developed from the Miami Isopycnic Coordinate Ocean Model (MICOM) using the theoretical foundation for implementing a hybrid coordinate system [*Bleck and Boudra*, 1981; *Bleck and Benjamin*, 1993].

[7] Three different eddy-resolving (1/12° equatorial resolution) HYCOM configurations are used. The basin scale Pacific HYCOM domain extends from 20°S to 65.8°N and from 98.9°E to 77.7°W. The Pacific HYCOM climatological simulation is forced with monthly averaged heat fluxes and monthly winds from the European Centre for Medium-Range Weather Forecasts [*ECMWF*, 1994], while the Pacific HYCOM interannual simulation is forced with daily averaged heat fluxes and six-hourly winds from ECMWF for the period 1979-2003. These two model experiments include realistic bottom topography and coastline geometry, which are based on a modified version of ETOP05 [*National Oceanic and Atmospheric Administration* (*NOAA*), 1986]. The model uses the 10 meter isobath as a land-sea boundary, includes 20 vertical coordinate layers, allows isopycnals intersecting sloping topography by allowing zero thickness layers, and does not include ocean data assimilation.

[8] The global model domain extends from 74°S to 90°N, and the nested GOC HYCOM domain extends from 118°W to 105°W and from 20°N to 32°N. The global and the GOC HYCOM configurations are identically forced with three-hourly winds and daily averaged heat fluxes from the Fleet Numerical Meteorology and Oceanography Center's Navy Operational Global Atmospheric Prediction System (NOGAPS) [*Rosmond et al.*, 2002], and they include monthly rivers and turbidity forcing [*Kara et al.*, 2005a, 2005b, 2005c]. Global and GOC HYCOM integrate during the period January 2003–June 2006. In addition, the models include realistic bottom topography and coastline geometry that are based on a modified version of the 1/30° NRL DBDB2 topography [http://www7320.nrlssc.navy.mil/DBDB2_WWW]. The models use the 5 meter isobath as a land-sea boundary. The models include 32 vertical layers, and do not include ocean data assimilation.

[9] It is important to clarify that extra effort was put into correcting any deficiencies in the ETOPO5 topography in the GOC region. Thus, the three different HYCOM configurations used in this study (Global, Pacific, and GOC) include the same topography (which is a modified version of the 1/30° NRL DBDB2 topography) in the GOC region. It is equally important to note that the increase in the vertical resolution from 20 layers in Pacific HYCOM to 32 layers in global and GOC HYCOM is due to the need to include more water masses in the global model. However, the vertical resolution change does not adversely affect any processes in the GOC.

[10] The boundary conditions for the nested GOC regional model are provided by global HYCOM. Nesting within HYCOM is a one-way off-line process (from the larger domain to the nested domain). During the nesting process the baroclinic modes are relaxed to the coarse outer grid solution via a relaxation buffer zone for temperature, salinity, pressure and horizontal velocity components. The barotropic mode is passed into the inner domain along approximations to characteristic lines for velocity and pressure [HYCOM User Guide: Wallcraft, 2003, available at http://hycom.rsmas.miami.edu/hycom-model/documentation.html]. The nesting parameters used in this study are: the boundary conditions are updated every 1-day, the relaxation buffer zone extends ~90 km (10 grid points), the relaxation time across the buffer zone is .1 to 1 days, and the barotropic and baroclinic modes are both included in the nested boundary conditions.

[11] Isolating the essential forcing that generates the summer of 2004 SGOC eddies is one the main objectives of this study. Thus, to isolate the effects of the local wind on the generation of the 2004 SGOC eddies, 1/12° resolution nested simulations were developed using the local GOC wind as the only forcing. Since in this particular simulation, the oceanic remote forcing (e.g. CTWs) is not included then all the processes forced in the GOC are due to the local wind forcing. Next, to isolate the effects of the oceanic remote forcing on the generation of the 2004 SGOC eddies, 1/12° resolution nested simulations were developed using oceanic remote forcing as the only forcing. Consequently, in this case, all the processes occurring in the GOC are due to the oceanic remote forcing. In addition, it should be noted that the 1/12° resolution is fine enough to resolve the SGOC eddies, the PEBC, the CTWs, and the Rossby radius of deformation of ~30 km of the GOC region. Thus, in the context of this study, it is not necessary to increase the horizontal resolution of the nested experiments.

3. Results and Discussion

[12] In this section HYCOM long-term means and snapshots are described and analyzed. Considering that the model analyzed results (1979–2006) include several thousand snapshots, the summer generation of the SGOC eddy train is presented and discussed using long-term means and two specific examples from the summers of 1999 and 2004. Those years were selected because both the satellite and hydrographic data used to validate the model results and the
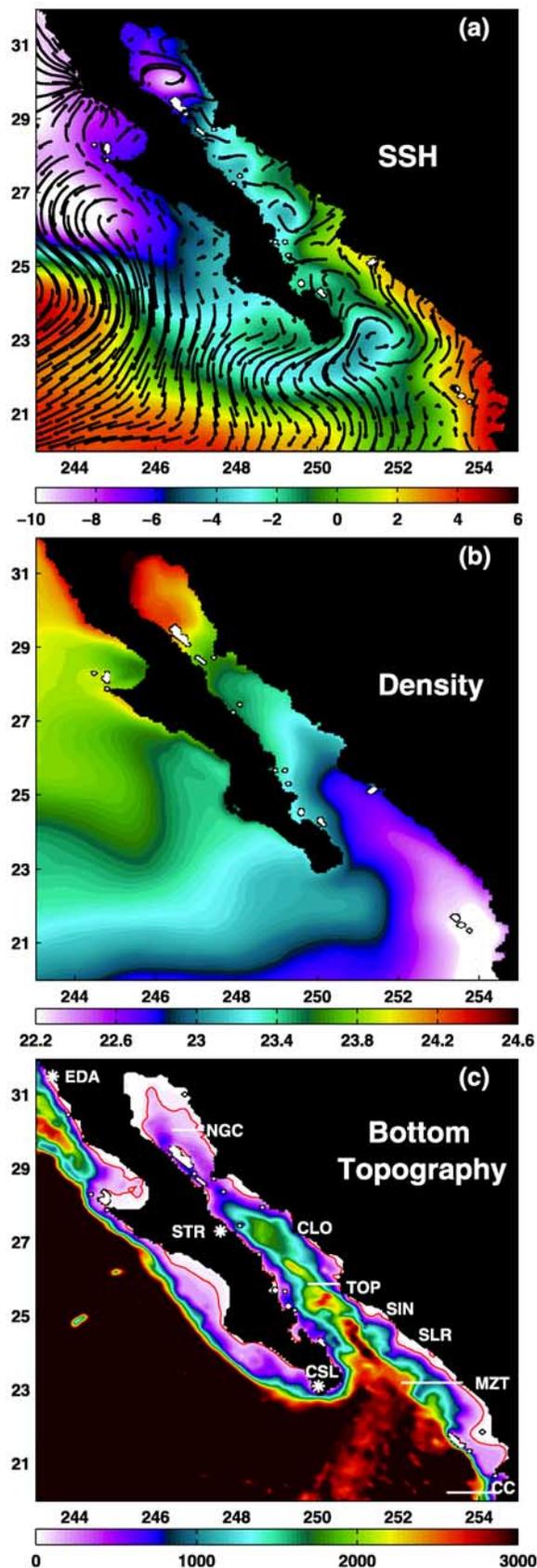
eddy generation hypothesis are already reported in the literature.

3.1. Mean and Monthly Circulation

3.1.1. Mean Circulation

[13] The mean currents along the west coast of Mexico are featured by a coastal poleward flow of ∼10 cm/s that extends ∼600 m in the water column and includes a coastal superficial maximum, which reaches the depth of ∼100 m at the entrance of the GOC. Furthermore, the coastal currents extend ∼1700 km in the alongshore direction (from Cabo Corrientes to the northern GOC), ∼100 km in the offshore direction, and decay poleward (Figures 1 and 2). These PEBC are formed by the Mexican Current that originates as the oceanic response to the local wind stress curl [*Zamudio et al.*, 2007], and by the Costa Rica Coastal Current that originates from the branch of the North Equatorial Counter Current, which turns northward near the Western Coast of the Americas [*Wyrtki*, 1966; *Zamudio et al.*, 2001; *Kessler*, 2006]. When these currents enter the GOC part of them remain adjacent to the coast, some start to meander, and the rest develop closed circulations (Figure 1a). The PEBC transport surface low-density waters, which are composed of surface low-salinity and high-temperature waters (Figures 1 and 2).

[14] At the entrance of the GOC the low-salinity coastal poleward currents are compensated by high-salinity coastal equatorward currents along the eastern coast of the Baja California Peninsula (Figure 2). There is a marked difference between the poleward inflow (broad, weak, low-salinity, and includes a coastal subsurface counter-current) and the equatoward outflow (narrow, strong, high-salinity, and it does not include a counter-current), and a marked similarity between the measured and simulated salinity pattern at the entrance of the GOC (compare Figure 2b with Figure 5b of *Castro et al.*, 2000). The model simulates the observed salinity maximum close to the eastern coast of the BCP and the division of this maximum, into surface (which extends from 0 to ∼60 m in both observations and simulations) and subsurface (which extends from ∼80 to ∼200 m in both observations and simulations) sub-maximums, and the broad low-salinity inflow which extends westward from the mainland side, centered at ∼80 (100) m in the observations (simulation). In addition, the simulated general pattern of the currents displayed in

Figure 1. 7-year mean of (a) sea surface height (color contours in cm) and top layer currents (arrow vectors), (b) density (σ_t) as determined from the climatologically forced Pacific HYCOM simulation, and (c) bottom topography (in meters) of the regional Gulf of California model. To help with the visualization of the topographic irregularities the 100-meters isobath (red contour) is added in panel (c). The positions of Cabo Corrientes (CC), Mazatlán (MZT), San Lorenzo River (SLR), Sinaloa River (SIN), Topolobampo (TOP), Cabo Lobos (CLO), Northern Gulf of California (NGC), Santa Rosalía (STR), Cabo San Lucas (CSL), and Ensenada (EDA) are indicated in panel (c). The upper-ocean (0-200 m) transport of Figure 5 was calculated along the four white zonal lines included in panel (c).

Figure 2a (a coastal poleward flow entering to the GOC along mainland Mexico, which is compensated by a coastal equatoward flow leaving the GOC along the eastern coast of the Baja California Peninsula) is in good agreement with the direct current measurements reported by *Collins et al.* [1997], and with the mean geostrophic currents reported by *Mascareñas et al.* [2004] and *Castro et al.* [2006].

3.1.2. Monthly Circulation

[15] The presence of the PEBC in the 7-year monthly means of SSH, surface currents, and meridional subsurface currents of Figures 3 and 4 shows a strong seasonal fluctuation and the existence of the PEBC throughout the year. The surface PEBC starts the year in a weakening mode that is evidenced by the SSH maximums at Cabo Corrientes (Topolobampo), which decays from $\sim$8 (2) cm in January to $\sim$4 ($-$10) cm in March (Figure 3a-3c). This January-February-March weakening pattern is not a surface phenomenon only, it is also reflected in the meridional subsurface currents (Figures 4a$-$4c). During January there is strong ($>$ 10 cm/s) concentrated outflow, extending from 0 to $\sim$500 m, along the Baja California side and a much broader inflow on the mainland side that includes a subsurface counter current (outflow) below the $\sim$200 m depth and close to the coast of mainland. By February both the inflow and outflow has weakened and the subsurface counter current along the mainland side has nearly disappeared. The weakening of the PEBC is more evident in March. In fact, this is the only month of the year when the outflow reaches the surface close to the coast of mainland Mexico. In addition, the first minimum of the year of the subsurface meridional currents is reached during March (Figure 4c). This January-February-March climatological weakening pattern is also evident in the upper-ocean (0-200 m) transport from Cabo Corrientes (outside of the GOC) to the Northen GOC (Figure 5).

[16] After the early year weakening pattern, the PEBC enter into a spring-summer strengthening mode that is evidenced by a progressive enhancement of the SSH along the coast of mainland Mexico from the south of Cabo Corrientes to the northern GOC, by a progressive strengthening of the subsurface meridional currents at the entrance of the GOC, and by a progressive intensification of poleward upper-ocean transport along mainland Mexico (Figures 3d$-$3g, 4d$-$4g, and 5).

[17] During its propagation, the PEBC encounter SGOC topographic irregularities which are localized at the capes at Topolobampo and Cabo Lobos and at the ridges extending offshore from the mouth of the San Lorenzo and Sinaloa Rivers (Figure 1c). Through April and May the currents round the capes to continue their advance as boundary currents (Figures 3d$-$3e). However, as the PEBC get stronger, by June-July when the currents encounter the capes and ridges, they start to meander and separate from the coast (Figures 3f$-$3g). Hence, by August the separation and meander of the currents is evidenced by the generation of three anticyclonic eddies, which are located to the west of the San Lorenzo River, and the Topolobampo and Cabo Lobos capes (Figure 3h). How are these eddies formed? A plausible answer to this question is discussed in the next paragraph.

[18] The distance between Cabo Lobos and Topolobampo and the ridge at the San Lorenzo River and Topolobampo is $\sim$240 km (Figure 1c). Similarly, the distance between the Cabo Lobos and Topolobampo eddies and the San Lorenzo and Topolobampo eddies is also $\sim$240 km (Figure 3h), which is also the alongshore wavelength of the meanders occurring during July (Figure 3g). That wavelength could be indicative of baroclinic instabilities. Baroclinic instabilities occur when perturbations grow by drawing energy from the available potential energy associated with sloping isopycnals [*Kundu*, 1990]. In the case of the PEBC these are characterized by a sharp rise of the SSH toward the coast (Figure 3). Although ocean currents are constantly exposed to perturbations of different wavelengths, they are predisposed to the growth of perturbations over a limited range of wavelengths. *Wright* [1980] and *Ikeda et al.* [1984] show that in a 3-layer system, the wavelength with the fastest growth rate is $\sim$6R_1 (where R_1 is the first baroclinic radius of deformation that is $\sim$30 km in the SGOC), which is $\sim$180 km in the SGOC. On the other hand, *Kundu* [1990] shows that in a 2-layer system, the wavelength with the fastest growth rate is $\sim$3.9 πR_1, which is $\sim$360 km in the SGOC. In the SGOC, the coastline and bottom topography impose a perturbation to the PEBC and that perturbation has a wavelength of $\sim$240 km, which according to theory has a wavelength in range of the wavelengths with the fastest grow rate for the SGOC. Hence, the interaction of the PEBC with the coastline and bottom topography triggers the meander of the PEBC. Next, the PEBC continues in an amplifying meander state, due to the potential growing of baroclinic instabilities, until the meander evolve into a series of eddies, generating the SGOC eddy train (Figure 3h).

[19] During September some of these eddies have reached the west coast of the SGOC and consequently, by October, the eddies rapidly weaken (Figures 3i$-$3j). Thus, the SGOC eddy train has a life period of 2-3 months. During October the subsurface meridional currents at the entrance of the GOC reach the second minimum of the year and that minimum is also evident in the upper-ocean transport from Cabo Corrientes to the northern GOC (Figures 3j, 4j, and 5). From October to December the PEBC goes into another strengthening mode (Figures 3j$-$3l, 4j$-$4l, and 5).

[20] The PEBC include two maximums of positive upper-ocean transport, one during May$-$June and the other during December (Figure 5). However, only one SGOC eddy train is formed during the year (Figure 3). If our hypothesis is correct and the interaction of the PEBC with the capes and ridges is the essential forcing of the SGOC eddies; then, it is expected to observe the generation of the SGOC eddy train during two different months through the year, one eddy train during summer and the other during winter. Our explanation for the formation of only one eddy train during the year is as follows. The positive pulse in May is locally strengthened by the weak downwelling favorable winds and the positive pulse in December is locally weakened by the stronger upwelling favorable winds. Since, during December the PEBC propagate against the wind.

[21] The simulation used to document the monthly variability of the PEBC and the generation of the SGOC eddy train was forced with climatological monthly winds. However, that simulation shows the formation of eddies along the SGOC during summer (Figure 3). Then, particular wind events and/or the propagation of interannual (2$-$7 years), intraseasonal (30$-$90 days), or high frequency (days) CTWs are not essential for the summer generation of the SGOC
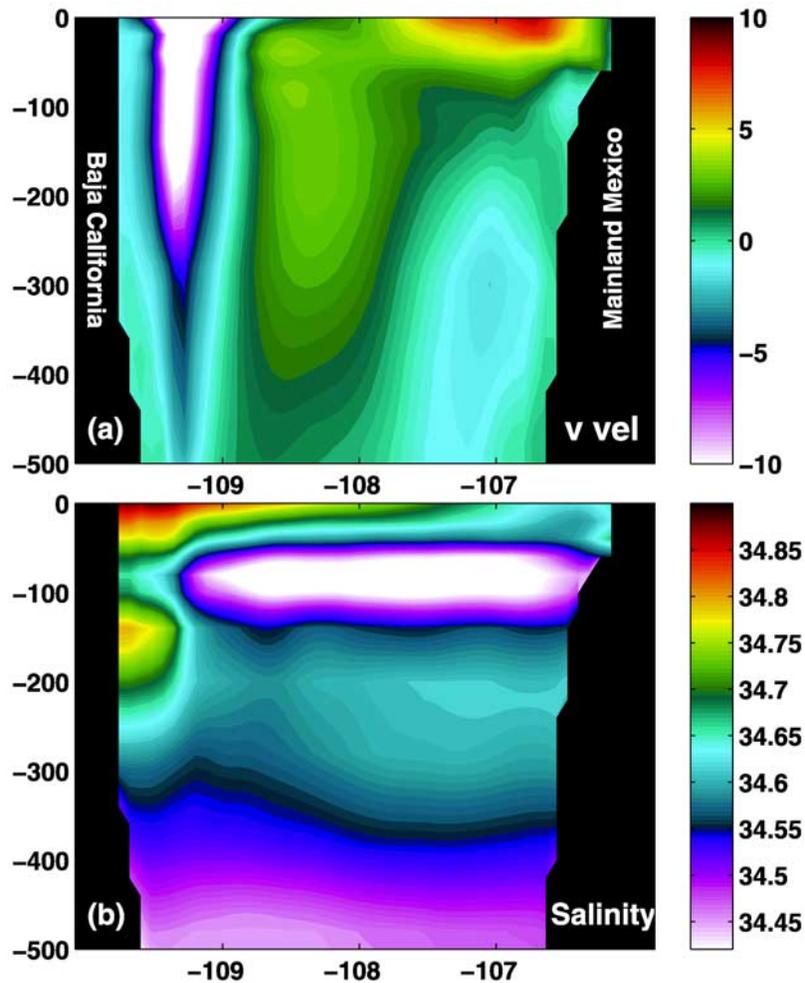
Figure 2. A 7-year mean of (a) meridional currents (color contours in cm/s), and (b) salinity (psu) as determined from the climatologically forced Pacific HYCOM simulation over a cross-section along a west-east line at ~23.2°N (close to the entrance of the GOC), which has the coast of the Baja California Peninsula on the west and the coast of mainland Mexico on the east. Positive currents indicate northward flow.

eddies, since CTWs in those frequency bands can not be generated by climatological monthly winds. Actually, the only CTWs included in the climatological simulation are the ones driven by the mean seasonal cycle. Thus, according with the results in Figures 1–5 the interaction of the summer intensified PEBC with the capes and ridges along the SGOC is the essential processes for the summer generation of the SGOC eddies. In addition, the local wind and/or CTWs can strength or weaken the PEBC and consequently enhance or depress the formation of the SGOC eddies (section 3.2).

3.2. Formation of Eddies During the Summers of 1999 and 2004

3.2.1. Summer of 1999

[22] Using SeaWIFS ocean color satellite measurements, *Pegau et al.* [2002] reported the summer surface circulation from the entrance of the GOC to 29°N. That circulation appears to be dominated by a series of eddies, which have an alternating sense of rotation. In particular, their 5 days chlorophyll images sequence for August-September 1999

clearly shows anticyclonic eddies emanating from the Capes at Topolobampo and Cabo Lobos and a less clear eddy emanating from the ridge at the San Lorenzo River (Figure 6).

[23] In accordance with the chlorophyll observations, the simulated SSH and surface currents for late August 1999 indicates a PEBC that has an associated sharp rise of the SSH toward the coast extending from Cabo Corrientes to the northern GOC (Figure 7). Both the SSH and the surface currents are strengthened by the presence of an equatorially-originated downwelling baroclinic CTW. The propagation of this specific CTW along the coast of the American Continent is displayed in the along coastal SSH versus time diagram of Figure 8, which shows the arrival of the CTW to the GOC during late August 1999. The poleward currents associated with this downwelling CTW intensified the local PEBC contributing to the generation and strengthening of the satellite-observed and model-simulated eddies (Figures 6 and 7).

[24] In concurrence with the observations, the simulated SSH and surface currents for late August 1999 include
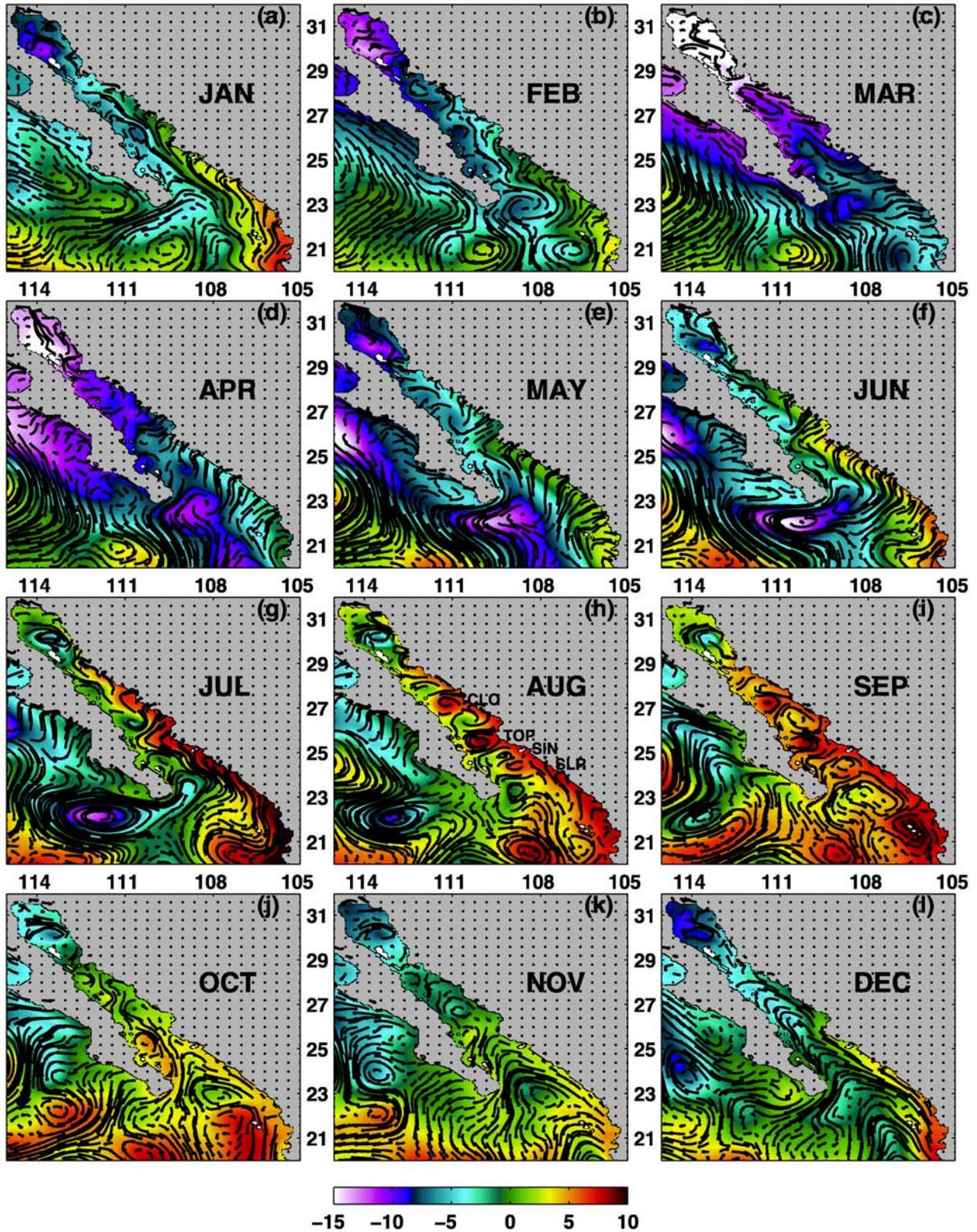
Figure 3. Monthly mean of sea surface sea surface height (color contours in cm) and surface currents (arrow vectors) as determined from the climatologically forced Pacific HYCOM simulation. Mean is based on 7 model years.
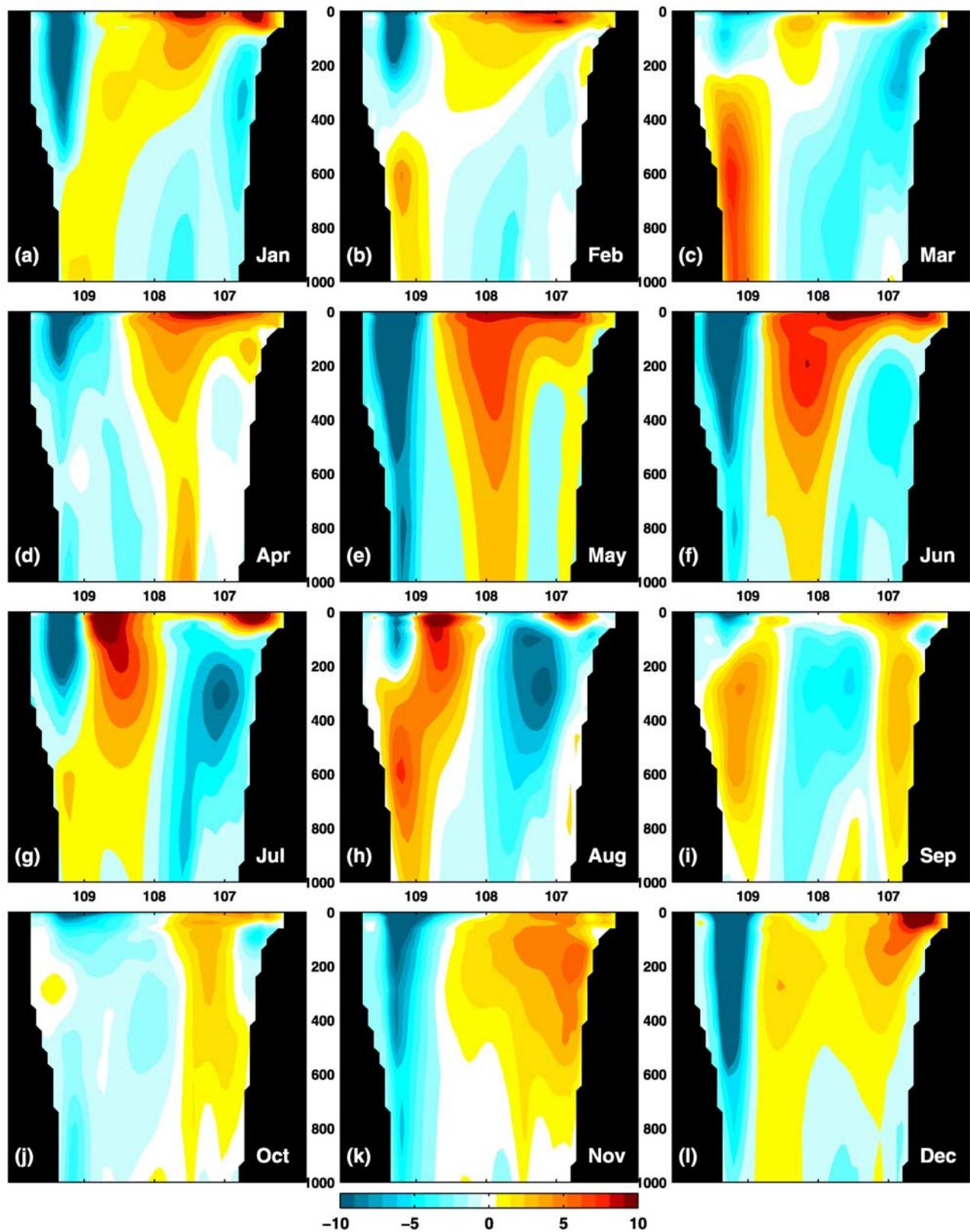
Figure 4. Monthly mean of meridional currents (color contours in cm/s) as determined from the 1/12° climatological Pacific HYCOM simulation over a cross-section along a west-east line at ∼23.2°N (close to the entrance of the GOC), which has the coast of the Baja California Peninsula on the west and the coast of mainland Mexico on the east. Positive currents indicate northward flow.
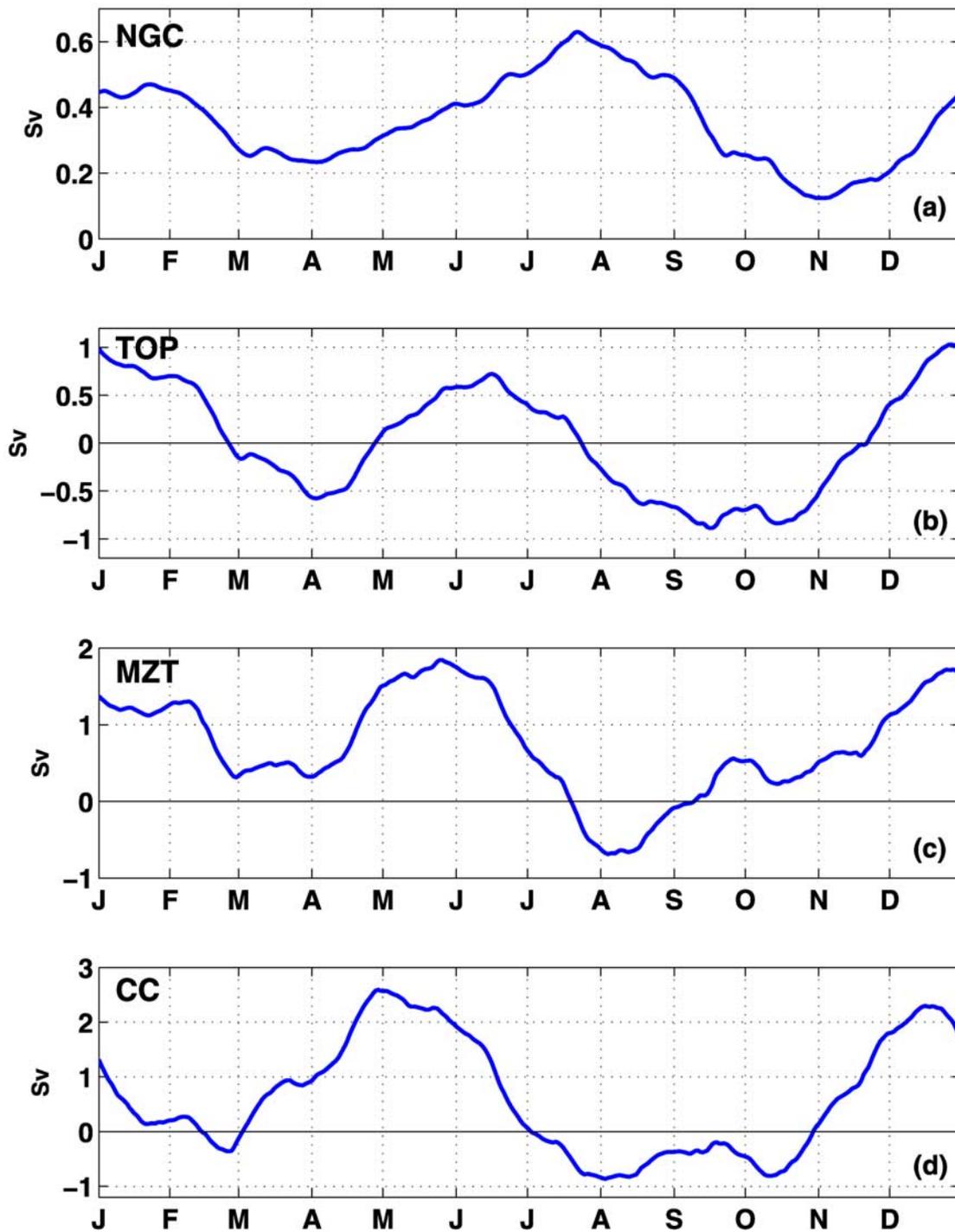
Figure 5. Annual upper-ocean (0–200 m) transport (in Sv) determined with the 1/12° climatologically forced Pacific HYCOM simulation over the four cross-sections indicated with white lines in Figure 1c. Positive transport indicates northward flow.

anticyclonic eddies to the west of Topolobampo and Cabo Lobos, and the ridge at the San Lorenzo River. These three simulated anticyclones show up as distinctive coastal signals, which are located in the same region as the observed ones. It is important to notice that the simulations used in this study do not include assimilation of any data, thus some differences in the location of the observed and simulated eddies are expected. Both the August 1999 simulated and observed anticyclonic eddies are co-located with the anti-cyclonic eddies of the 7 year monthly climatology, support-ing the hypothesis of a coastally imposed perturbation, which forces the coastal currents to separate from the coast, meander, and evolve generating a large number of eddies having an impact in the 7 year monthly climatology of Figure 3h.
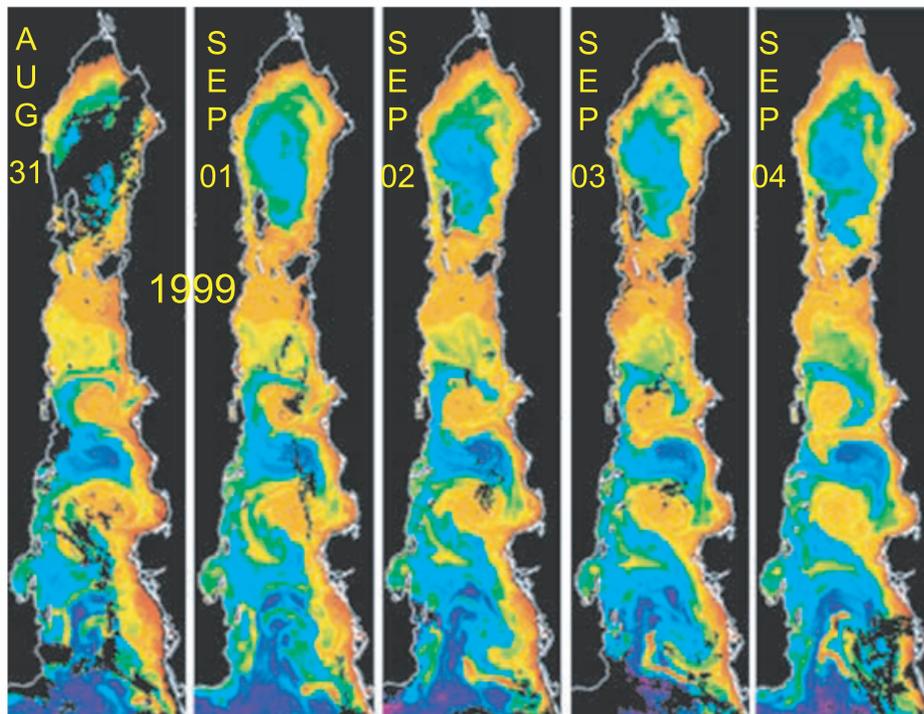
Figure 6. SeaWiFS chlorophyll images for five different dates in August-September 1999. Blue and green (yellow and red) colors represent low (high) chlorophyll concentrations. Adapted from *Pegau et al.* [2002].

[25] The SSH and surface currents of Figure 7 include cyclonic eddies located to the north and south of the Cabo Lobos, Topolobampo and San Lorenzo anticyclonic eddies, resembling the observed ones (see Figure 1 from *Pegau et al.*, 2002). In addition, Figure 7 includes a cyclonic eddy, filling the northern GOC. That cyclonic eddy is also displayed in the chlorophyll observations of Figure 6. Furthermore, the local currents and the anticyclonic eddies were intensified by the passage of a high-frequency short-wavelength downwelling CTW generated by Hurricane Greg [http://www.nhc.noaa.gov]. That CTW is displayed as the maximum SSH anomaly in Figure 8.

[26] In summary the August 1999 equatorially-generated downwelling baroclinic CTW intensified the PEBC that interact with the capes at Tapolobampo and Cabo Lobos, and the ridge at the San Lorenzo River, generating meanders that amplify and evolve into a series of eddies along the SGOC. Later, Hurricane Greg generated a second downwelling CTW, which strengthened the PEBC and the anticyclonic eddies.

3.2.2. Summer of 2004

[27] The SSH climatological monthly means of Figure 3 shows the formation of the SGOC eddies during July–August. The SST in the GOC ranges from 29°C to 33°C during July and August [*Zamudio et al.*, 2004]. Thus, the SGOC warm-core anticyclonic eddies exist in a region where the surrounding waters are also warm. Consequently, the July–August high SST makes it difficult to discern the eddies' thermal signature in satellite SST images [*Paden et al.*, 1991]. Nevertheless, the MODAS SST [*Barron and Kara*, 2006] shows the existence of anticyclonic warm-core

eddies (which are characterized by a radius of ∼65 km) along the axis of the SGOC during early August 2004 (Figure 9a). In addition, the MODAS SST includes a strong annual cycle, which is well simulated (correlation coefficient of 0.97) by HYCOM (Figure 9b). The high frequency variability (Figure 9c), which is due to the passage of tropical storms and CTWs that variability is also well simulated by HYCOM (correlation coefficient of 0.58). As described in the introduction section, the existence of the SGOC eddies during August 2004 has been validated by the direct hydrographic observations of *Castro et al.* [2007] and the drifters observations of *Lavín et al.* [2007].

[28] Figure 10 is a diagram of along coastal SSH versus time, as simulated by Global HYCOM. It shows the equatorial Pacific as the generation region of a CTW, which amplifies as it propagates poleward along the coast of the North American continent, arriving to the GOC during June 2004, with a SSH anomaly of >20 cm, and a SST anomaly of ∼2°C (Figure 9c). It is distinguished by an increment of the northward upper-ocean transport of ∼2 Sv at the entrance of the GOC and is measured by the sea level tide gauges at Balboa, Manzanillo, Santa Rosalia, Cabo San Lucas, and Ensenada (Figure 11). It is hypothesized that this specific CTW strengthened the PEBC and contributed to the generation the warm core eddies of Figure 9a. To test this hypothesis, the effects of the CTW on the generation of the eddies are isolated by forcing the regional model with oceanic remote forcing only. Next, to evaluate the effects of the local wind on the generation of the eddies, the regional model is forced with the local winds only. Finally, a third simulation is forced with both local and remote
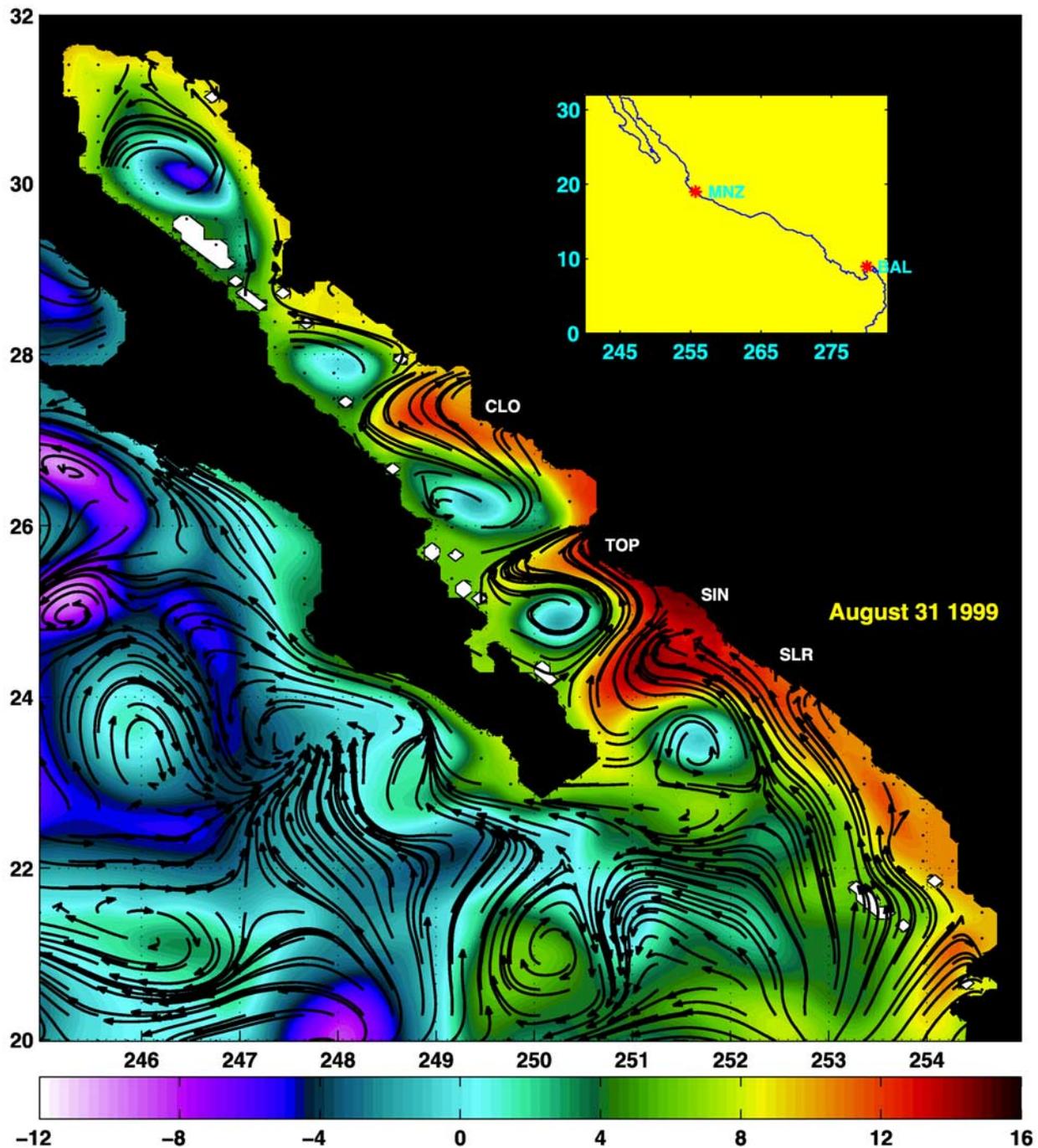
Figure 7. Sea surface height (color contour in cm) and top layer currents (arrow vectors) for August 31, 1999 as determined by the 1/12° interannually forced Pacific HYCOM simulation. The yellow insert includes the North American continent coastline from 0°N to 32°N along which the along-coastal versus time sea surface height diagrams of Figures 8 and 10 were calculated. The positions of Balboa (BAL) and Manzanillo (MNZ) are indicated.

forcings. To avoid any model results difference due to differences in the initial conditions, the three simulations were started (on May 3, 2004) from the same initial condition that was provided by global HYCOM.

[29] Three sequences of snapshots showing the June 2004 CTW as trigger, generator, and modulator of the summer 2004 eddies are presented in Figures 12, 13, and 14. On May 03, 2004 the along coast SSH anomaly from Cabo

Corrientes to the NGOC is <-5 cm, the currents speed is $\sim$15 cm/s (not shown), eddies with a radius of $\sim$15 km are located to the west of Topolobampo and Cabo Lobos, and no eddies are located to the west of the mouth of the San Lorenzo River (Figure 12a, 12f, and 12k). At this time, the kinetic energy and the salinity fields include upper-ocean maximums, which decrease rapidly with depth (Figures 13a, 13d, 13g, 14a, 14d, and 14g). In addition, the influence of
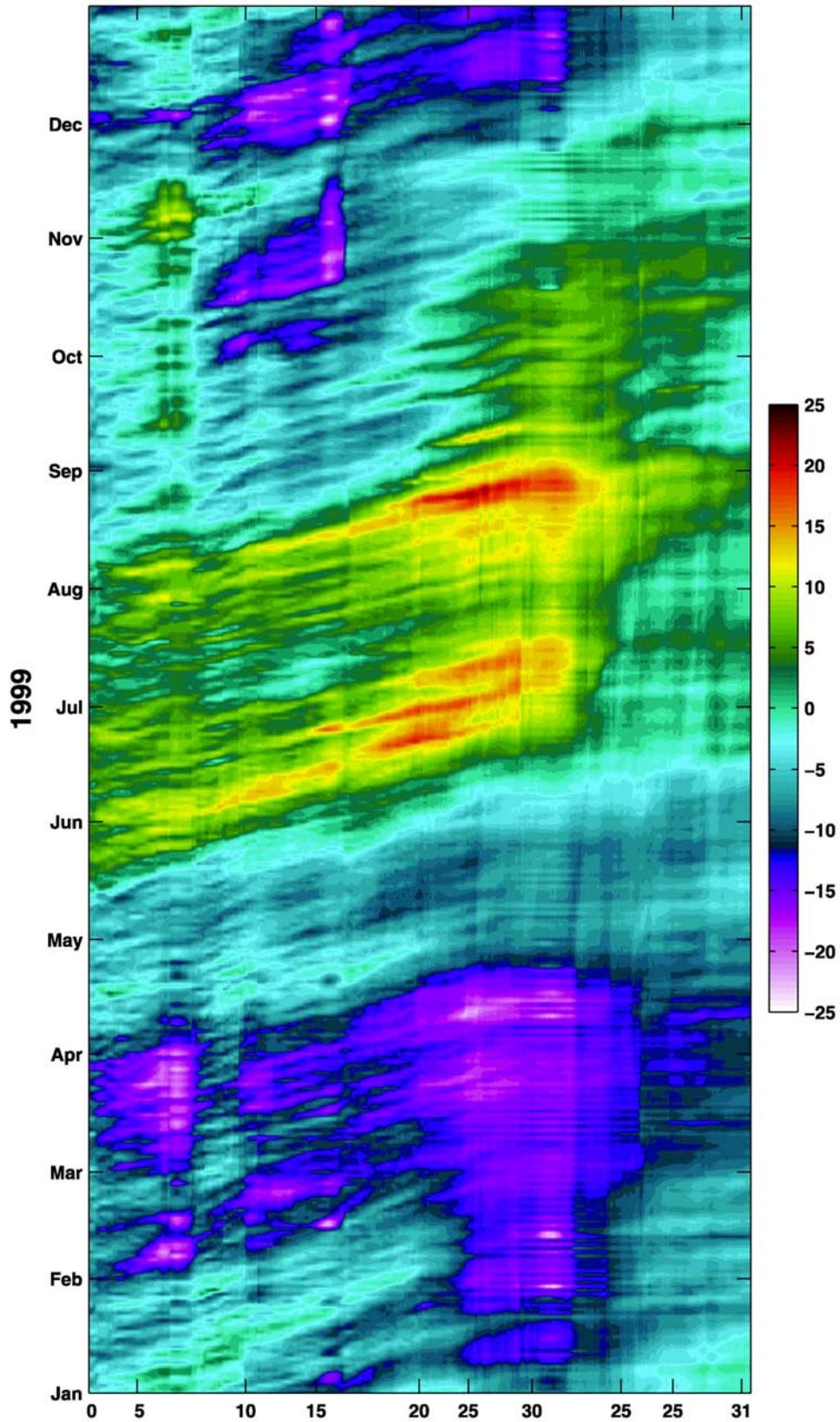
Figure 8. Sea surface height (in centimeters) time series for 1999 from 1/12° interannually forced Pacific HYCOM simulation along the coast of the North American continent from 0°N to 32°N as shown in Figure 7. Latitudes along the coast are indicated, including the three times when the coastline reach the latitude of 25°N.
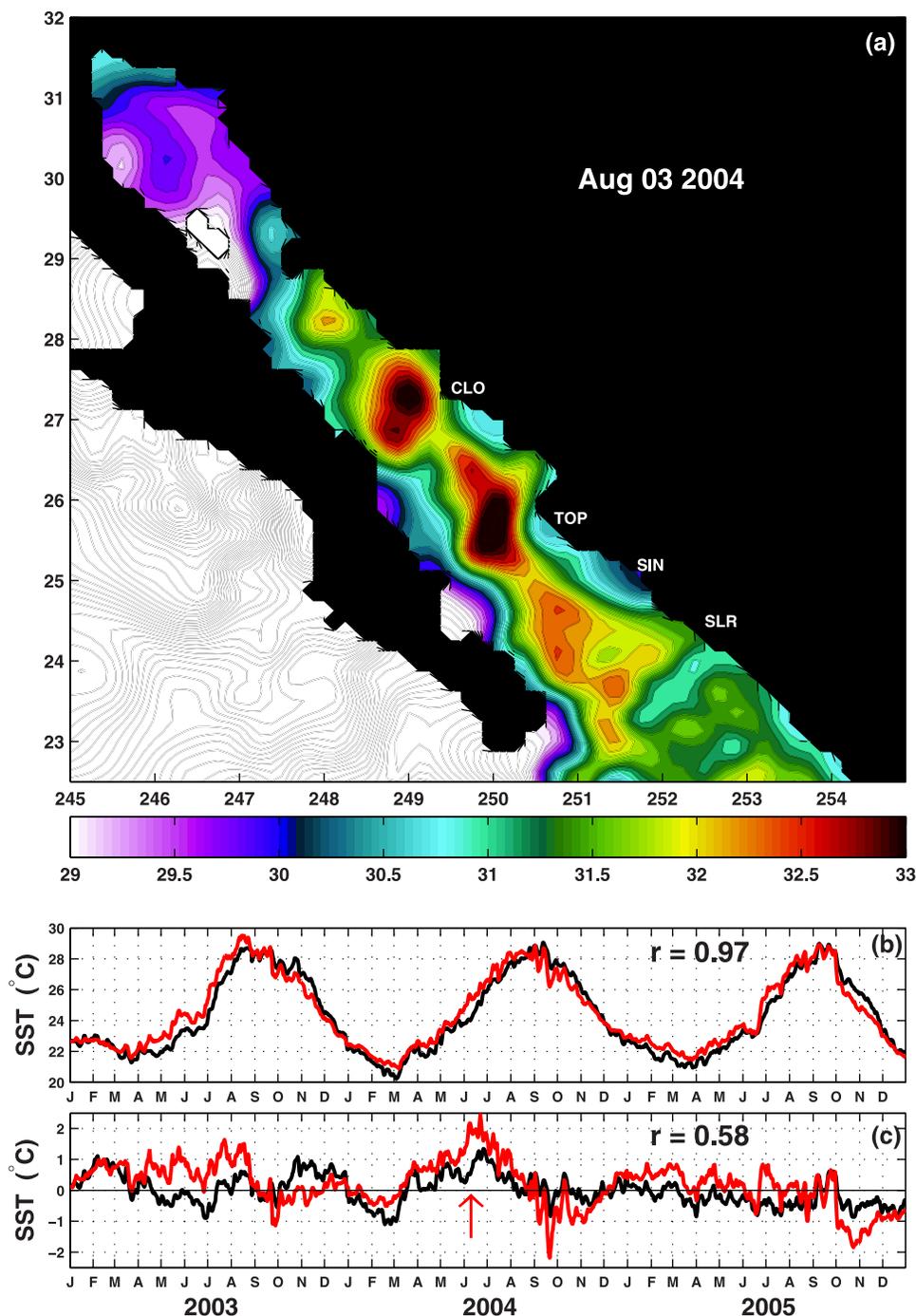
Figure 9. (a) Sea surface temperature (SST) snapshot (in °C) for August 3 2004 as determined from MODAS. Time series of GOC domain wide SST average: (b) before removing the annual cycle, (c) after removing the annual cycle as determined from MODAS (black lines) and from 1/12° nested interannually forced GOC HYCOM simulation forced with local and remote forcings (red lines). The correlation coefficients between the time series in panels (b) and (c) are indicated. The ~2°C increment of May-June 2004 is indicated with a red arrow in panel (c).

the California Current and the rivers (Santiago, San Pedro, Piaxtla, Ameca, and Acaponeta located to the south of the cross-section of Figure 13) in the salinity field is evident by the salinity minimum with center close to 230 m and 110°W (Figures 13a, 13d, and 13g). Forty five days later, upon the arrival of the strong downweling CTW to the GOC, the

along coast SSH anomaly, current's speed, and northward upper-ocean transport increase to >20 cm, >50 cm/s, and ~2 Sv, respectively and no anticyclonic eddy activity can be recognized in the area (Figures 12b, 12g, and 12l). However, the influence of the Topolobampo and Cabo Lobos capes on the CTW is reflected by the separation of the CTW
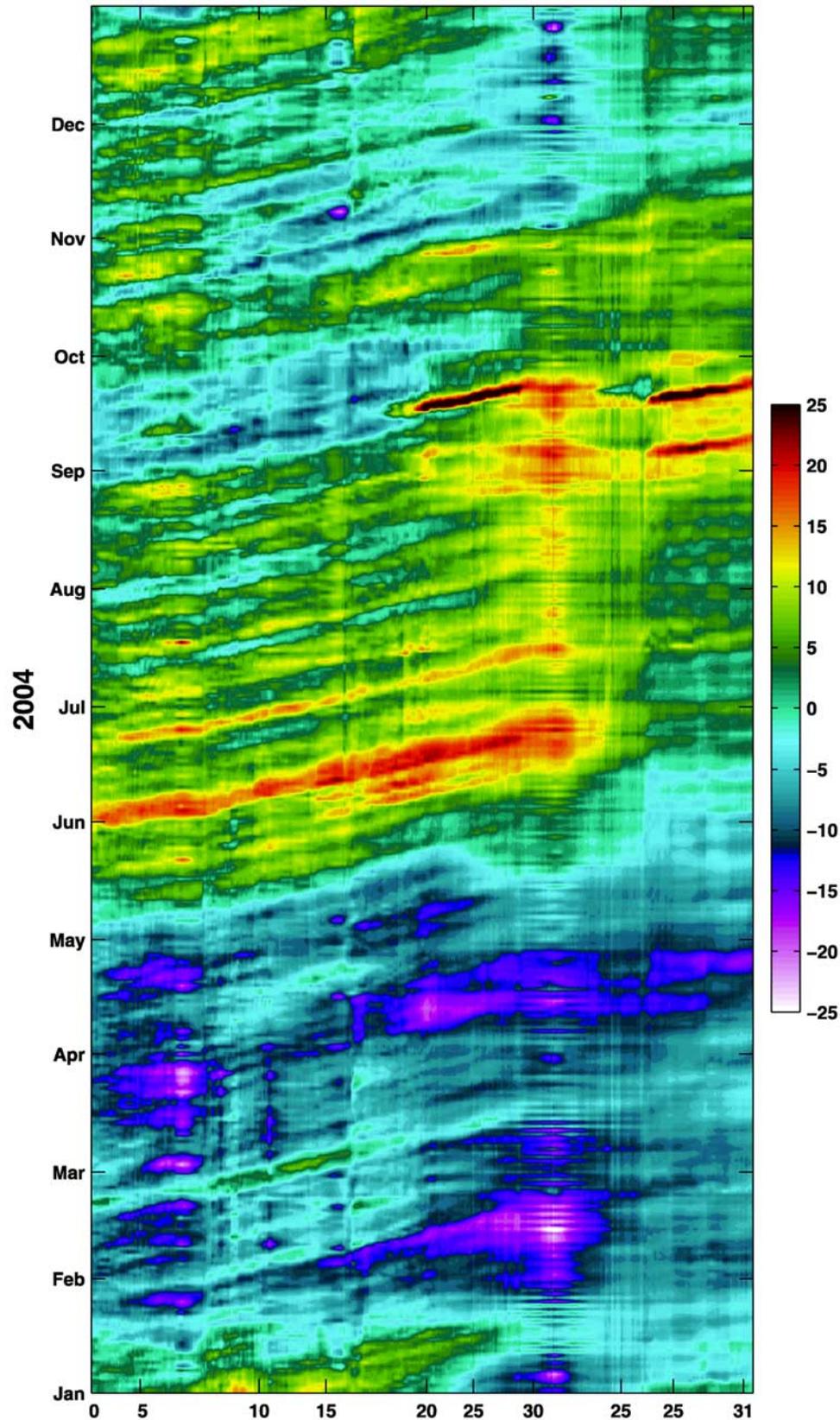
Figure 10. Sea surface height (in centimeters) time series for 2004 from 1/12° interannually global HYCOM simulation along the coast of the North American continent from 0°N to 32°N as shown in Figure 7. Latitudes along the coast are indicated, including the three times when the coastline reach the latitude of 25°N.
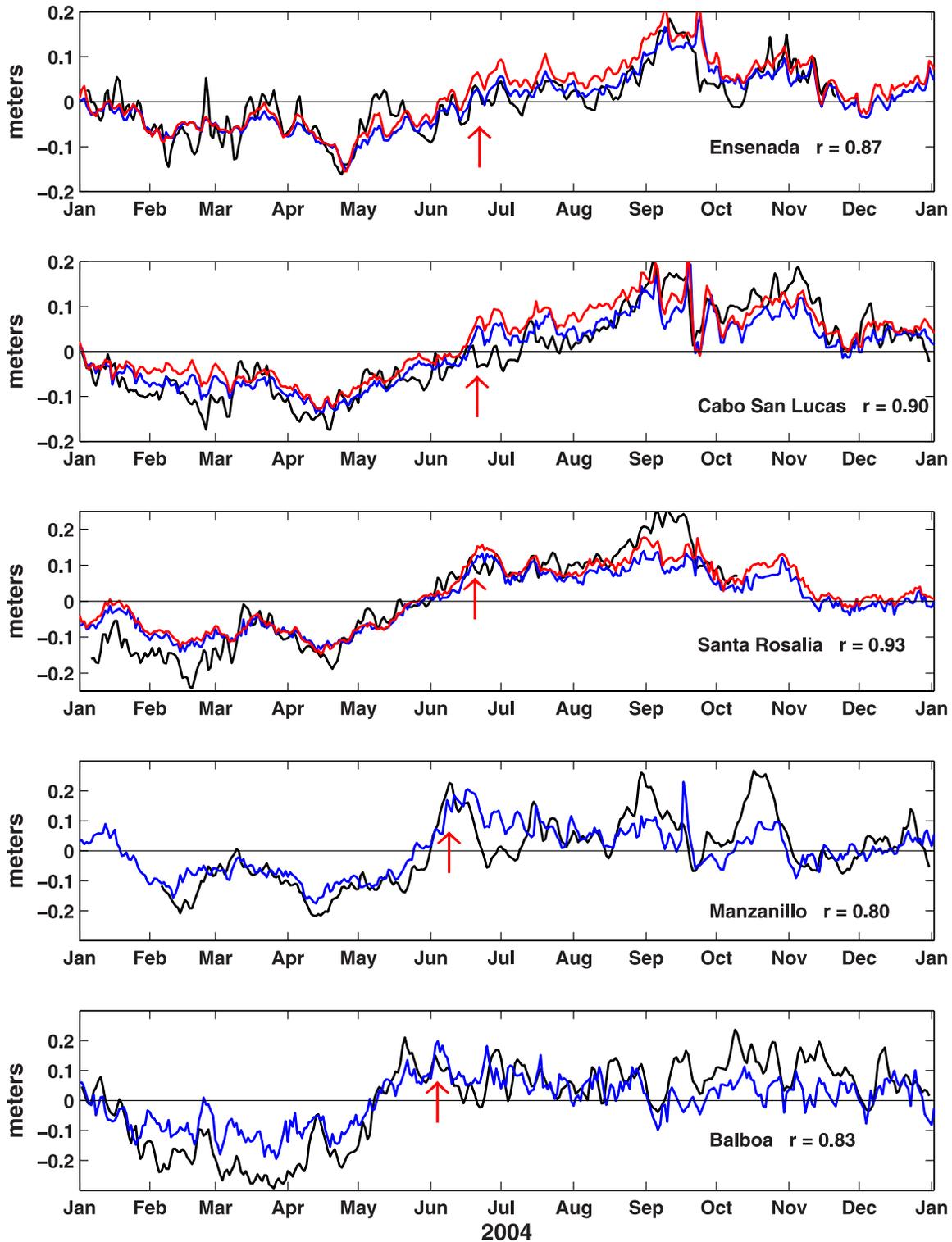
Figure 11. Time series of sea surface height anomaly at Balboa, Manzanillo, Santa Rosalía, Cabo San Lucas, and Ensenada. The observed data (black line) has been detided and corrected for atmospheric pressure loading. The blue (red) lines were simulated using the 1/12° interannually forced global HYCOM experiment (the 1/12° nested interannually forced GOC–HYCOM experiment forced with local plus remote forcings). The correlation coefficients between the observations and simulations are indicated. The June 2004 sea surface height increment is indicated with red arrows.
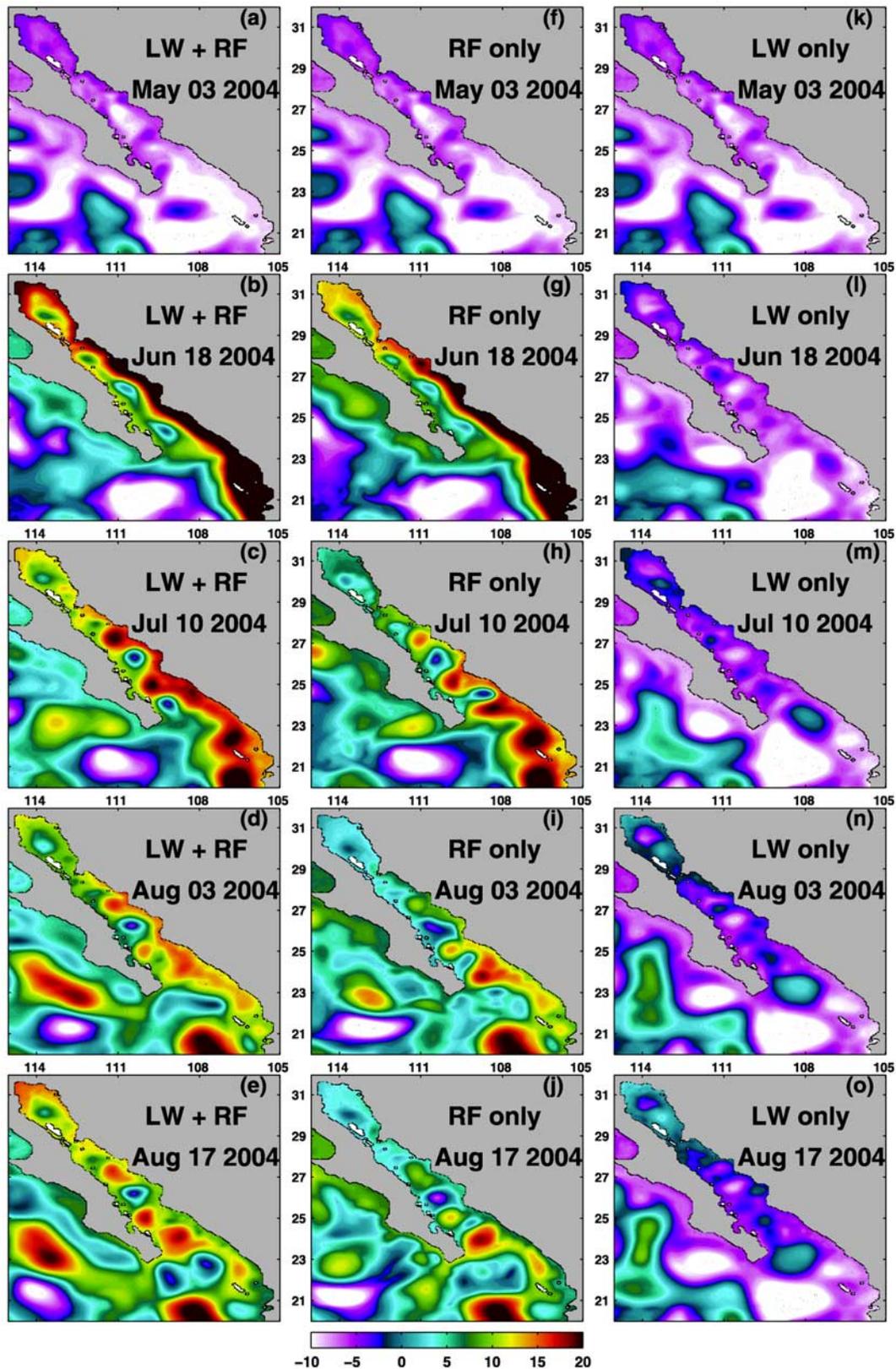
Figure 12. Sea surface height anomaly snapshots (color contours in cm) for five different dates during spring–summer of 2004. Simulated with the 1/12° nested interannually forced GOC–HYCOM experiments: (a)–(e) with local plus remote forcings, (f)–(j) with remote forcing only, and (k)–(o) with local forcing only.
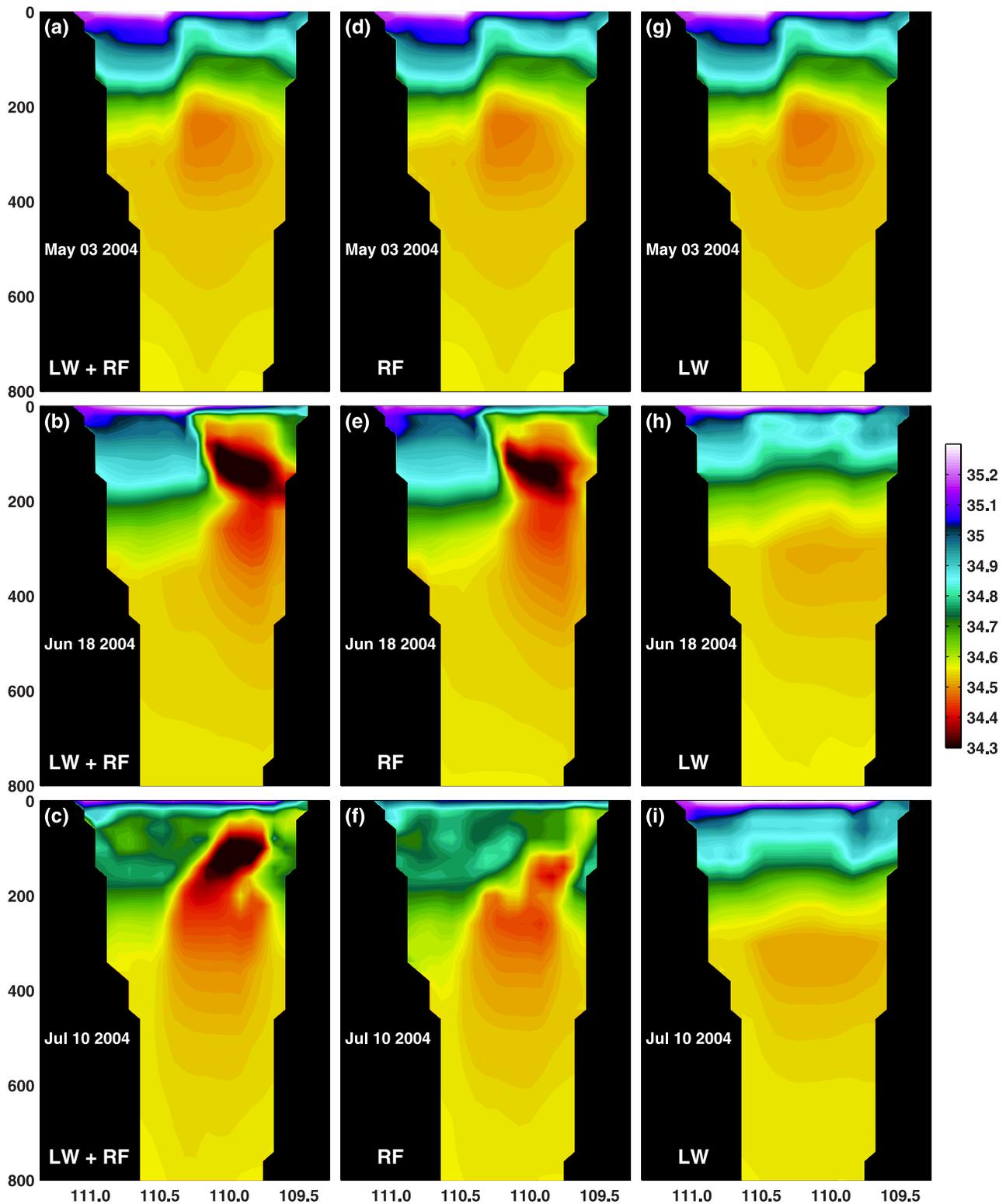
Figure 13. Salinity snapshots (color contours in psu) for three different dates during spring–summer of 2004. Simulated with the 1/12° nested interannually forced GOC–HYCOM experiments over a cross–section at the latitude of Topolobampo. (a)–(c) Forced with local plus remote forcings, (d)–(f) forced with remote forcing only, and (g)–(i) forced with local forcing only.
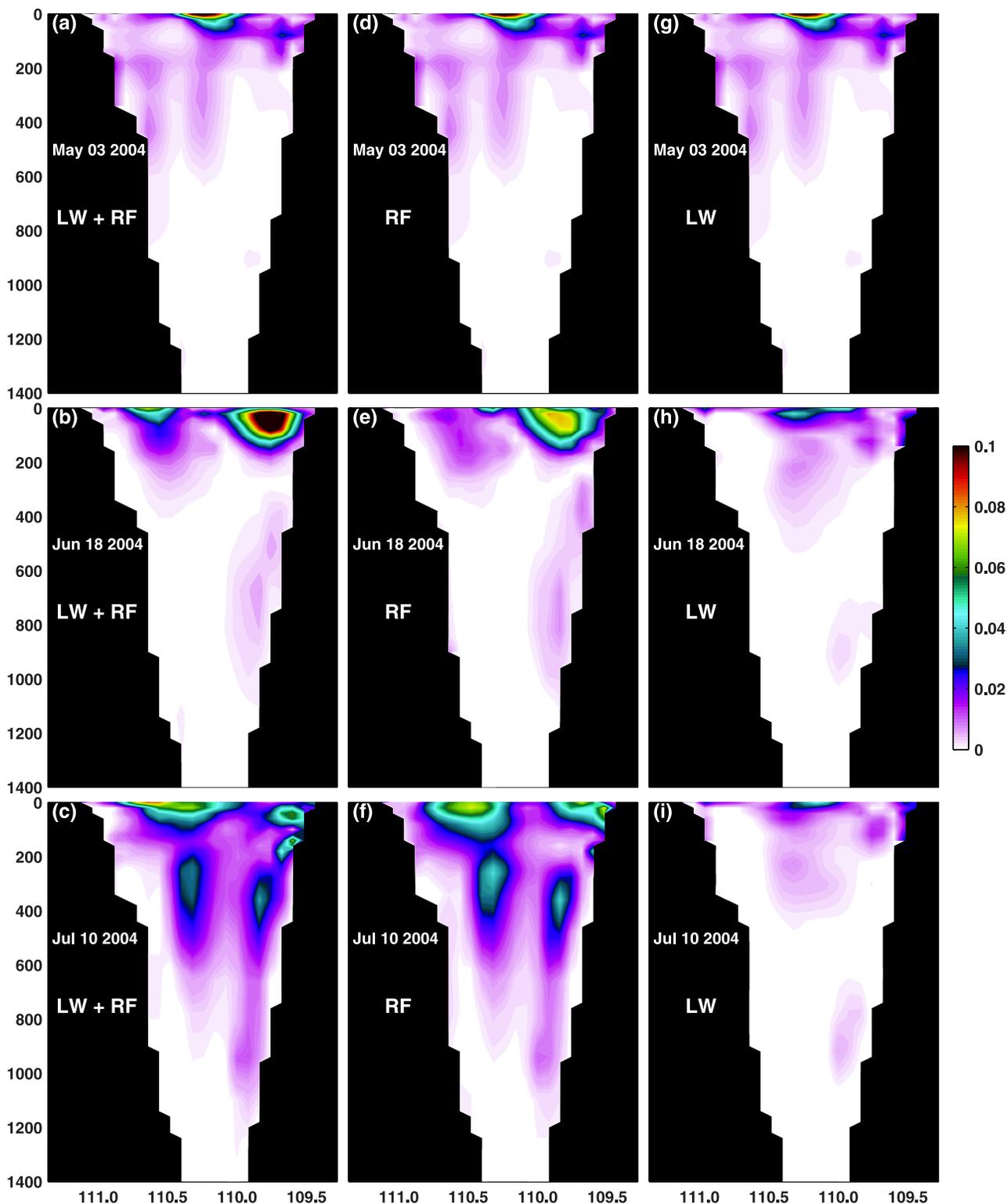
Figure 14. Kinetic energy snapshots (color contours in m^2/s^2) for three different dates during spring–summer of 2004. Simulated with the 1/12° nested interannually forced GOC–HYCOM experiments over a cross–section at the latitude of Topolobampo. (a)–(c) Forced with local plus remote forcings, (d)–(f) forced with remote forcing only, and (g)–(i) forced with local forcing only.

from the coast (Figures 12b and 12g). At the same time, the local wind stress curl forced the Mexican Current raising the along coast SSH ∼3 cm from Cabo Corrientes to the Northern GOC (Figure 12l). In addition, this CTW generates a strong salinity front that is clearly displayed in the simulations including oceanic remote forcing (Figures 13b–13c, and 13e–13f), and no salinity front is included in the simulation lacking of the oceanic remote forcing (Figures
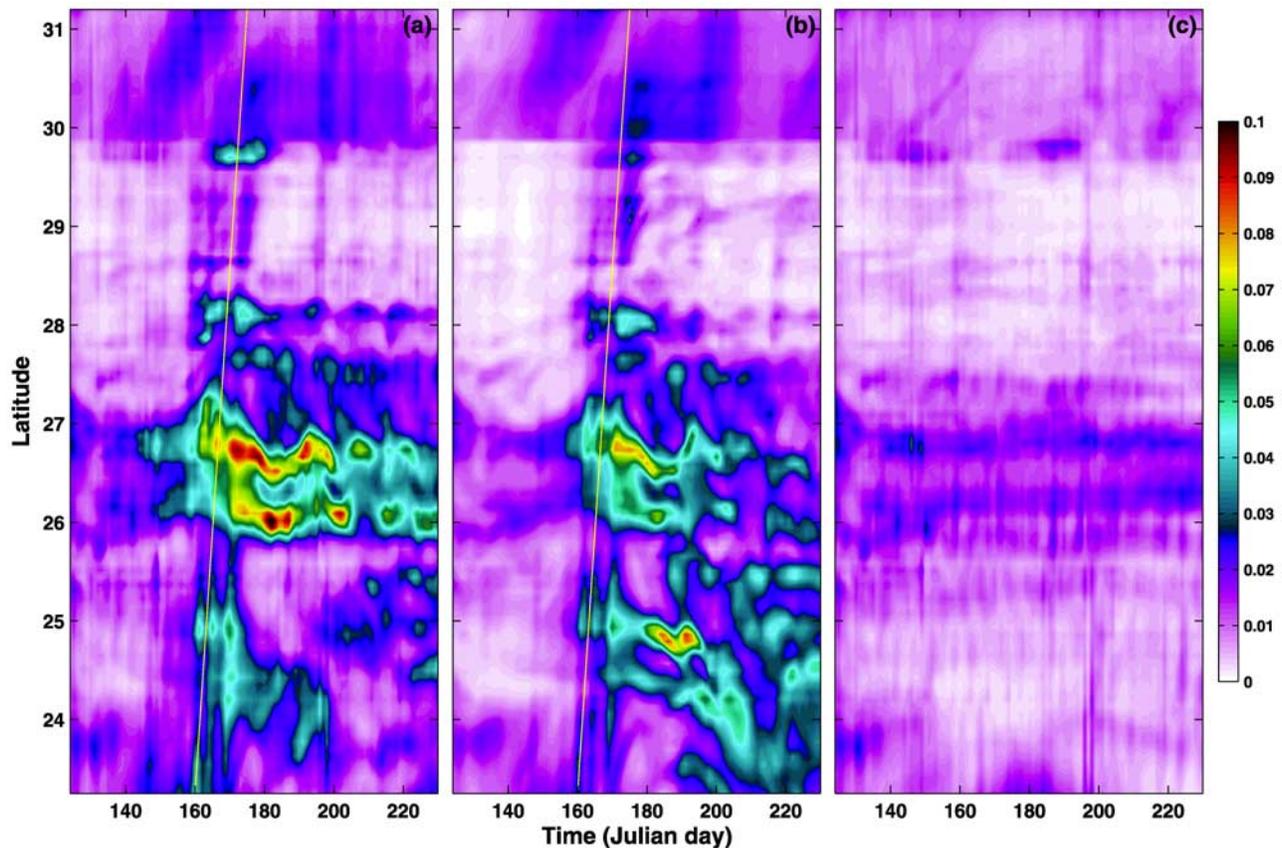
Figure 15. Longitudinal–averaged along GOC upper–ocean (0–200 m) kinetic energy (m²/s²) versus time for the period May 3, 2004 – August 17, 2004, simulated with the 1/12° nested interannually forced GOC–HYCOM experiments: (a) with local plus remote forcings, (b) with remote forcing only, and (c) with local forcing only. The thin yellow line in panels (a) and (b) is plotted to help with the visualization of the propagation of the summer of 2004 CTW.

13h–13i). Furthermore, this CTW generates a strong upper-ocean maximum in the kinetic energy field (Figures 14b and 14e). By July 10, the separation of the CTW from the coast and its meandering have evolved into anticyclonic eddies, which are characterized by a SSH anomaly, radius, swirl velocity, and depth of >15 cm, ∼65 km, >45 cm/s, ∼1000 m respectively (Figures 12c, 12h, 14c, and 14f). Note the similarity between the kinetic energy fields of the two simulations including the oceanic remote forcing and how the kinetic energy fields extends in the water column to depths of ∼1000 m, a direct result of the passage of the CTW and the formation of this particular eddy (Figure 14). In contrast, the local wind generated shallow and weak eddies to the southwest of Topolobampo and Cabo Lobos (Figures 12m and 14i). A month later the CTW has exited the GOC, the eddies have propagated to the west, and the eddies' SSH has decreased as a result of the interaction of the eddies with the west coast of the GOC and the absence of their main forcing (the CTW) (Figures 12d–12e, and 12i–12j). Note the agreement between the simulated and observed eddies depth of ∼1000 m (Figures 14c and 14f).

[30] To provide some insight on the generation of the eddies by the summer of 2004 CTW, longitudinal-averaged along GOC upper-ocean (0–200 m) kinetic energy versus time diagrams are displayed in Figure 15. The diagrams of Figure 15a and 15b show the propagation of the CTW along the GOC. Associated with the passage of the CTW by SGOC there is a significant increase in the kinetic energy, as a result of the generation of the eddies. That energy increase is well delimited in space (from ∼27°N, which is the latitude of Cabo Lobos to the entrance of the GOC) and time (during and after the passage of the CTW) in the simulations including oceanic remote forcing, and absent in the simulation forced with local wind only. Although, the main generator of the summer of 2004 eddies is the CTW, it should be noted that the wind by itself generated coastal currents (Figures 12k–12l), and those currents interact with the ridges and capes generating eddies (Figure 12m). However, these wind-generated eddies are shallower and weaker than those observed by *Castro et al.* [2007] and those generated by the oceanic remote forcing.

[31] The observations and simulations analyzed in this study indicate that the SGOC anticyclonic eddies are oceanic-remotely-forced features, which are formed in basically the same coastal geographical location (on the northwest of Topolobampo, Cabo Lobos, and San Lorenzo River) each time they are generated. That suggests predominantly (partially) deterministic (nondeterministic) processes involve in the creation of these eddies. Hence, to provide some insight on the deterministic nature of the separation,
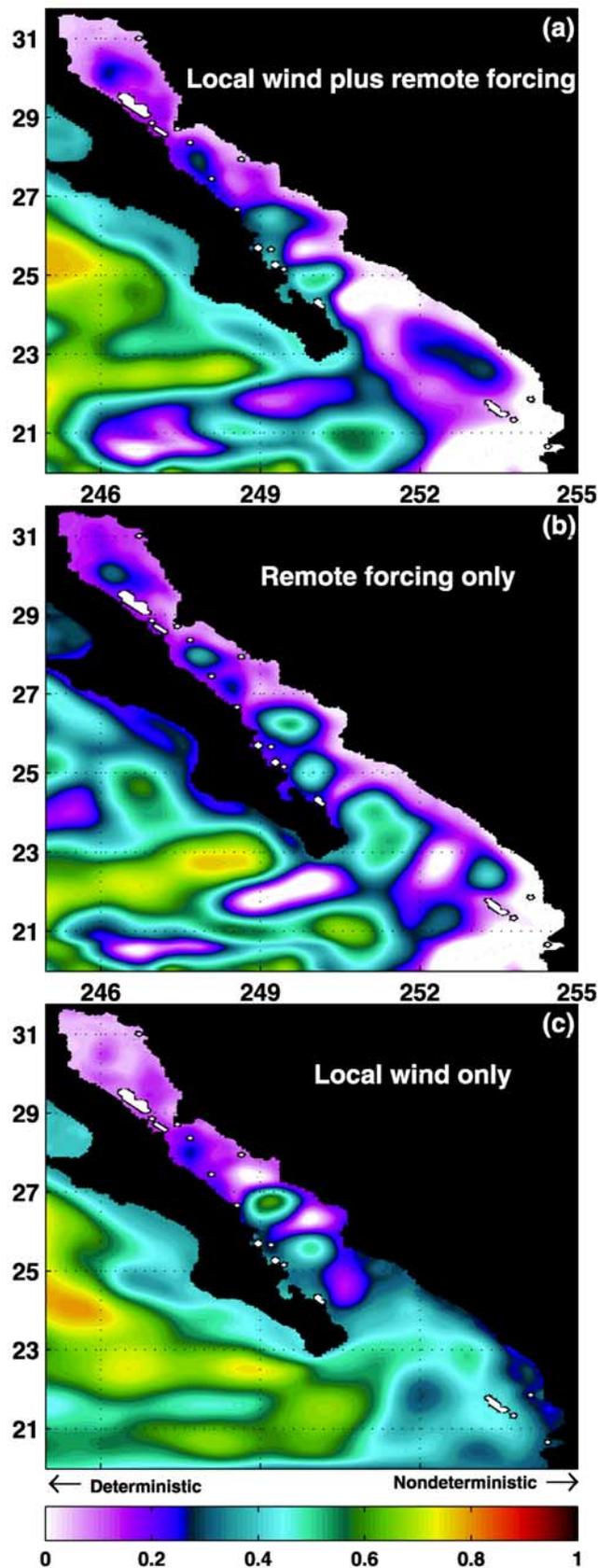
meander, and reattachment of the currents from the coast, the deterministic (which is considered as a direct response to the atmospheric, topographic, and remote forcings), and nondeterministic (which is attributed to nonlinear mesoscale flow instabilities) regions of the GOC are calculated in the next section.

3.3. Deterministic Versus Nondeterministic SSH Variability in the Gulf of California

[32] In order to assess the degree of determinism in the experiments used in this study, three ensembles of seven simulations (in each ensemble) were integrated over the period 2003–2005. The 3-year period of integration permits the generation of several SGOC eddy trains. The seven simulations included in the first ensemble were forced with both local and remote forcings. To isolate the effects of the remote forcing on the deterministic and nondeterministic response of the GOC, the simulations included in the second ensemble used remote forcing only. To isolate the effects of the local winds, the simulations included in the third ensemble used local forcing only.

[33] In each ensemble the simulations differ only in their initial states (30 days apart). Since these simulations differ only in initial state, any differences between them can be attributed to nondeterministic differences in both the initial conditions and the evolution of the simulations. *Metzger et al.* [1994], *Metzger and Hurlburt* [2001], *Melsom et al.* [2003], *Hogan and Hurlburt* [2005], and *Zamudio and Hogan* [2008] used a technique to separate the variability of a scalar variable into two components. The deterministic component is the direct response to the atmospheric forcing, the bottom topography and the coastline geometry, and the remote forcing provided by the global scale model through the boundaries of the regional nested model. The nondeterministic component is due to nonlinear mesoscale flow instabilities.

[34] *Metzger*'s *et al.* [1994] technique is summarized as follows. First, the long-term mean (2003-2005) SSH is computed over the seven realizations. This mean is then removed from each daily record of the individual simulations to form seven time series of SSH anomaly fields (η). At each grid point, the temporally corresponding records of the seven realizations are averaged ($\bar{\eta}$) and deviations ($\eta' = \eta - \bar{\eta}$) are computed about the mean comprised of all realizations. These are then combined and averaged as follows:

$$\overline{\eta^2} = \bar{\eta}^2 + \overline{\eta'^2}$$

where the bar represents the average over all realizations. Averaging over the same period as the mean formed from all realizations, as was done here ensures that the temporal average of the deterministic anomalies is zero. Assuming $\bar{\eta}$ is

Figure 16. Deterministic versus nondeterministic sea surface height variability for the GOC. Low and high values indicate high and low degree of determinism. These results are based on three ensembles of seven simulations for each ensemble simulated with the 1/12° nested interannually forced GOC–HYCOM experiments: (a) using local plus remote forcings, (b) using remote forcing only, and (c) using local forcing only.

accurately defined by a large number of realizations, then, the left-hand side represents the total SSH variability and the right-hand side represents the SSH variability due to atmospheric, topographic, and remote forcings, plus the variability due to flow instabilities. Next, each component of the equation is divided by the total SSH variability ($\overline{\eta^2}$) to determine the fraction of the SSH variability due to either atmospheric-topographic-remote forcings or flow instabilities. Since the accuracy of this calculation depends on the number of ensemble members, then the fraction of variability was computed for 2, 3, 4, 5, 6, and 7 realizations. The quantitative and qualitative differences between the results of these calculations (maps) become progressively smaller as more simulations are included, with six or seven realizations sufficient for near convergence of this methodology.

[35] The fraction of nondeterministic variability of SSH for the regional GOC model clearly shows the deterministic character of the coastal regions along the mainland coast of the GOC that is mainly due to the remote forcing provided by the PEBC and the passages of CTWs (Figures 16a–16b) and the deterministic character of the NGOC due to the local wind (Figure 16c). Note that in the two ensembles forced with remote forcing the capes at Topolobampo and Cabo Lobos and the ridges extending offshore from the entrance of the San Lorenzo and Sinaloa Rivers are located inside of deterministic regions indicating that the processes driving the SSH variability in these regions (including eddy formation) have a deterministic nature. In contrast, the SSH variability along the west coast of the GOC is more nondeterministic than that along the east coast of the GOC. That is due to: (1) the absence of a permanent/quasi-permanent coastal current (like the PEBC), and (2) the weaker CTWs propagating along the west coast of the GOC compared with the stronger CTWs propagating along the east coast of the GOC. During their northward propagation, the CTWs weaken at the shelf-break located north of Cabo Lobos, and at this location a portion of the CTWs propagate to the northern GOC and the other portion reverses direction and propagates southward along the west coast of the GOC. Overall, the presence of the PEBC and the strong transient events associated with the propagation of CTWs along the mainland coast of the GOC imprint the deterministic character of the SSH variability.

4. Summary and Concluding Remarks

[36] The summer generation of the SGOC eddies is studied using three different eddy resolving (1/12° equatorial resolution) configurations (global, Pacific basin scale, and GOC nested regional scale) of HYCOM. As a first step, a monthly climatology of the currents of the GOC was created utilizing the Pacific configuration. Hence, this climatology shows: (1) the observed pattern of the currents at the entrance of the GOC, which is featured by the low-salinity PEBC entering to the GOC along the coast of mainland Mexico and the high-salinity coastal equatorward currents leaving the GOC along the eastern coast of the Baja California Peninsula, (2) the GOC's response to both local and remote forcings, (3) the strong monthly variability of the PEBC, including maximums in the northward upper-ocean transport during May-June and December, and (4) the separation and meander of the deterministic PEBC from the

capes at Topolobampo and Cabo Lobos, and the ridge at the San Lorenzo River and the consequently summer generation of the SGOC eddies. Since the climatology was generated from a simulation forced with climatological monthly winds, then particular wind events and/or the arrival of interannual, intraseasonal, or high frequency CTWs are not crucial for the summer generation of the SGOC eddies. However, CTWs can strengthen the PEBC and contribute to the generation of stronger SGOC eddies, as illustrated by two particular CTWs arriving to the GOC during the summers of 1999 and 2004. In these two events, the interannually forced model-simulated eddies are validated with the satellite-observed eddies of *Pegau et al.* [2002], and with the MODAS SST eddies for the summers of 1999 and 2004, respectively.

[37] The propagation of the equatorially-originated summer of 2004 CTW was registered by the coastal sea level tide gauges located inside and outside of the GOC, showing the capability (model-data comparisons with correlation coefficients from 0.80 to 0.93) of HYCOM to simulate this CTW. The crucial (unnecessary) role of this CTW (the local wind) on the intensification of the northward upper-ocean transport, the strengthening of the PEBC, and the subsequently generation of the SGOC eddies was demonstrated forcing the nested regional GOC model with oceanic remote forcing only (local wind only).

References

Badan-Dangon, A., C. J. Koblinsky, and T. Baumgartner (1985), Spring and summer in the Gulf of California, observations of surface thermal patterns, *Oceanol. Acta*, *8*, 13–22.

Barron, C. N., and A. B. Kara (2006), Satellite-based daily SST's over the global ocean, *Geophys. Res. Lett.*, *33*, LI5603, doi:10.1029/2006GL026356.

Baumgartner, T. R., and N. Christensen Jr. (1985), Coupling of the Gulf of California to large-scale interanual climatic variability, *J. Mar. Res.*, *43*, 825–848.

Beier, E. (1997), A numerical investigation of the annual variability of the Gulf of California, *J. Phys. Oceanog.*, *27*, 615–632.

Beier, E., and P. Ripa (1999), Seasonal Gyres in the Northern Gulf of California, *J. Phys. Oceanog.*, *29*, 305–311.

Bleck, R. (2002), An oceanic general circulation model framed in hybrid isopycnic-cartesian coordinates, *Ocean Model.*, *37*, 55–88.

Bleck, R., and D. B. Boudra (1981), Initial testing of a numerical ocean circulation model using a hybrid (quasi-isopycnic) vertical coordinate, *J. Phys. Oceanogr.*, *11*, 755–770.

Bleck, R., and S. G. Benjamin (1993), Regional weather prediction with a model combining terrain-following and isentropic coordinates. Part 1: Model description, *Mon. Weather Rev.*, *121*, 1770–1785.

Bray, N. A. (1988), Thermohaline circulation in the Gulf of California, *J. Geophys. Res.*, *93*, 4993–5020.

Castro, R., A. S. Mascareñas, R. Durazo, and C. A. Collins (2000), Seasonal variation of the salinity and temperatura at the entrance of the Gulf of California, Mexico, *Ciencias Marinas*, *26*(4), 561–583.

Castro, R., R. Durazo, A. Mascareñas, C. A. Collins, and A. Trasviña (2006), Thermohaline variability and geostrophic circulation in the southern portion of the Gulf of California, *Deep-Sea Res. I*, *53*, 188–200.

Castro, R., M. F. Lavín, E. Beier, and A. Amador (2007), Structure of mesoscale eddies in the southern Gulf of California during cruise NAME-2 (August 2004), *Eos Trans. AGU*, *88*(23), Jt. Assem. Suppl., Abstract U24A-05.

Christensen, N., Jr., R. de la Paz, and G. Gutierrez (1983), A study of sub-inertial waves off the west coast of Mexico, *Deep-Sea Res.*, *30*, 835–850.

Collins, C. A., N. Garfield, A. S. Mascareñas, M. G. Spearman, and T. Rago (1997), Ocean currents across the entrance to the Gulf of California, *J. Geophys. Res.*, *102*(C9), 20,927–20,936.

Enfield, D. B., and J. S. Allen (1983), The generation and propagation of sea level variability along the Pacific coast of Mexico, *J. Phys. Oceanogr.*, *13*, 1012–1033.

European Center for Medium-range Weather Forecasts (ECMWF) (1994), The description of the ECMWF/WCRP level III −A global atmospheric data archive, report, 72 pp., Reading, England.

Hogan, P. J., and H. E. Hurlburt (2005), Sensitivity of simulated circulation dynamics to the choice of surface wind forcing in the Japan/East Sea, *Deep Sea Res., Part II*, *52*, 1464–1489.

Ikeda, M., L. A. Mysak, and W. J. Emery (1984), Seasonal variability in meanders of the California Current system off Vancouver Island, *J. Geophys. Res.*, *89*, 3487–3505.

Kara, A. B., A. J. Wallcraft, and H. E. Hurlburt (2005a), A new solar radiation penetration scheme for use in ocean mixed layer studies: An application to the Black Sea using a fine resolution HYbrid Coordinate Ocean Model (HYCOM), *J. Phys. Oceanogr.*, *35*, 13–32.

Kara, A. B., A. J. Wallcraft, and H. E. Hurlburt (2005b), How does solar attenuation depth affect the ocean mixed layer? Water turbidity and atmospheric forcing impacts on the simulation of seasonal mixed layer variability in the turbid Black Sea, *J. Climate*, *18*, 389–409.

Kara, A. B., A. J. Wallcraft, and H. E. Hurlburt (2005c), Sea surface temperature sensitivity to water turbidity from simulations of the turbid Black Sea using HYCOM, *J. Phys. Oceanogr.*, *35*, 33–54.

Kessler, W. S. (2006), The circulation of the eastern tropical Pacific: A review, *Progress Oceanogr.*, *69*, 181–217.

Kundu, P. K. (1990), *Fluid Mechanics*, 638 pp., Academic Press, Orlando, Fla.

Lavín, M. F., P. P. Niiler, A. Amador, R. Castro, and E. Beier (2007), Surface velocity patterns in the Gulf of California from satellite-tracked drifters, *Eos Trans. AGU*, *88*(23), Jt. Assem. Suppl., Abstract OS51D-02.

López, M., L. Zamudio, and F. Padilla (2005), Effects of the 1997-1998 El Niño on the exchange of the northern Gulf of California, *J. Geophys. Res.*, *110*, C11005, doi:10.1029/2004JC002700.

Marinone, S. G. (2003), A three-dimensional model of the mean and seasonal circulation of the Gulf of California, *J. Geophys. Res.*, *108*(C10), 3325, 10.1029/2002JC001720.

Martínez, J. A., and J. S. Allen (2004a), A modelling study of coastal-trapped wave propagation in the Gulf of California. Part I: Response to remote forcing, *J. Phys. Oceanogr.*, *34*, 1313–1331.

Martínez, J. A., and J. S. Allen (2004b), A modelling study of coastal-trapped wave propagation in the Gulf of California. Part II: Response to idealized forcing, *J. Phys. Oceanogr.*, *34*, 1332–1349.

Mascareñas, A. S., Jr., R. Castro, C. A. Collins, and R. Durazo (2004), Seasonal variation of geostrophic velocity and heat flux at the entrance of the Gulf of California, Mexico, *J. Geophys. Res.*, *109*, C07008, doi:10.1029/2003JC002124.

Melsom, A., E. J. Metzger, and H. E. Hurlburt (2003), Impact of remote oceanic forcing on Gulf of Alaska sea levels and mesoscale circulation, *J. Geophys. Res.*, *108*(C11), 3346, doi:10.1029/2002JC001742.

Merrifield, M. A., and C. D. Winant (1989), Shelf Circulation in the Gulf of California: a description of the variability, *J. Geophys. Res.*, *94*, 18,133–18,160.

Merrifield, M. A. (1992), A comparison of long coastal-trapped wave theory with remote-storm-generated wave events in the Gulf of California, *J. Phys. Oceanogr.*, *22*, 5–18.

Metzger, E. J., H. E. Hurlburt, G. A. Jacobs, and J. C. Kindle (1994), Hindcasting wind-driven anomalies using reduced-gravity global ocean models with 1/2° and 1/4° resolution, *NRL Tech. Rep. 9444*, 21 pp., Nav. Res. Lab., Stennis Space Center, Miss.

Metzger, E. J., and H. E. Hurlburt (2001), The nondeterministic Nature of Kuroshio Penetration and Eddy Shedding in the South China Sea, *J. Phys. Oceanogr.*, *31*, 1712–1732.

National Oceanic and Atmospheric Administration (NOAA) (1986), ETO-PO5 digital relief of the surface of the earth, National Geophysical Data Center, Washington, D.C., Data Announcement 86-MGG-07.

Paden, C. A., M. R. Abboutt, and C. D. Winant (1991), Tidal and atmospheric forcing of the upper ocean in the Gulf of California 1. Sea surface temperature variability, *J. Geophys. Res.*, *96*, 18,337–18,359.

Palacios, E., E. Beier, M. F. Lavín, and P. Ripa (2002), The effect of winter mixing on the circulation of the Northern Gulf of California, *J. Phys. Oceanogr.*, *32*, 705–728.

Palacios-Hernández, E., L. Carrillo, M. F. Lavín, L. Zamudio, and A. García-Sandoval (2006), Hydrography and circulation in the Northern Gulf of California during winter of 1994-1995, *Cont. Shelf Res.*, *26*, 82–103.

Pegau, W. S., E. Boss, and A. Martinez (2002), Ocean color observations of eddies during the summer in the Gulf of California, *Geophys. Res. Lett.*, *29*(9), 1295, doi:10.1029/2001GL014076.

Ripa, P. (1997), Toward a physical explanation of the seasonal dynamics and thermodynamics of the Gulf of California, *J. Phys. Oceanog.*, *27*, 597–614.

Rosmond, T. E., J. Teixeira, M. Peng, T. F. Hogan, and R. Pauley (2002), Navy Operational Global Atmospheric Predictions System (NOGAPS): Forcing for ocean models, *Oceanography*, *15*(1), 99–108.

Wright, D. G. (1980), On the stability of a fluid with specialized density stratification, II, Mixed baroclinic-barotropic instability with application to the Northeast Pacific, *J. Phys. Oceanogr.*, *10*, 1037–1322.

Wyrtki, K. (1966), Oceanography of the eastern equatorial Pacific Ocean, *Oceanogr. Mar. Biol. Annu. Rev. Rev.*, *4*, 33–68.

Zamudio, L., A. P. Leonardi, S. D. Meyers, and J. J. O'Brien (2001), ENSO and Eddies on the Southwest Coast of Mexico, *Geophys. Res. Lett.*, *28*(1), 13–16.

Zamudio, L., H. E. Hurlburt, E. J. Metzger, and O. M. Smedstad (2002), On the evolution of coastally trapped waves generated by Hurricane Juliette along the Mexican West Coast, *Geophys. Res. Lett.*, *29*(23), 2141, doi:10.1029/2002GL014769.

Zamudio, L., E. J. Metzger, H. E. Hurlburt, and P. J. Hogan (2004), On the monthly variability in the Gulf of California, *Eos Trans. AGU*, *84*(52), Ocean Sci. Meet, Suppl., Abstract OS31D-02.

Zamudio, L., H. E. Hurlburt, E. J. Metzger, and C. Tilburg (2007), Tropical wave-induced oceanic eddies at Cabo Corrientes and the María Islands, Mexico, *J. Geophys. Res.*, *112*, C05048, doi:10.1029/2006JC004018.

Zamudio, L., and P. J. Hogan (2008), Nesting the Gulf of Mexico in Atlantic HYCOM: Oceanographic Processes Generated by Hurricane Ivan, *Ocean Modelling*, *21*(3–4), 106–125, doi:10.1016/j.ocemod.2007.12.002.

————————————

P. Hogan, E. J. Metzger, and L. Zamudio, Naval Research Laboratory, Ocean Modeling and Prediction, Stennis Space Center, Code 7323, MS 39529, USA. (luiz.zamudio@nrlssc.navy.mil)